



ACADEMIC  
PRESS

Available online at [www.sciencedirect.com](http://www.sciencedirect.com)

SCIENCE @ DIRECT®

Journal of Solid State Chemistry 175 (2003) 133–145

JOURNAL OF  
SOLID STATE  
CHEMISTRY

<http://elsevier.com/locate/jssc>

# NaPdPS<sub>4</sub> and RbPdPS<sub>4</sub>: systems with infinite straight $\frac{1}{\infty}[\text{PdPS}_4]^-$ chains soluble in polar solvents and the structure of cubic RbPdPS<sub>4</sub>{Rb<sub>0.33</sub>P<sub>0.4</sub>S<sub>2.23</sub>O<sub>x</sub>}

Servane Coste,<sup>a</sup> Jason Hanko,<sup>b</sup> Martine Bujoli-Doeuff,<sup>a</sup> Guy Louarn,<sup>a</sup> Michel Evain,<sup>a</sup> Raymond Brec,<sup>a</sup> Bruno Alonso,<sup>c</sup> Stéphane Jobic,<sup>a</sup> and Mercouri G. Kanatzidis<sup>b,\*</sup>

<sup>a</sup>Institut des Matériaux Jean Rouxel, CNRS UMR 6502, 2 rue de la Houssinière, BP 32229, 44322 Nantes cedex 3, France

<sup>b</sup>Department of Chemistry and Center for Fundamental Materials Research, Michigan State University, 320 Chemistry Building, East Lansing, MI 48824, USA

<sup>c</sup>Centre de Recherches sur la Physique des Hautes Températures, CNRS UPR 4212, 1D avenue de la Recherche Scientifique, 45071 Orléans cedex 02, France

Received 23 September 2002; received in revised form 28 February 2003; accepted 6 March 2003

## Abstract

The synthesis, crystal structures, chemical and spectroscopic properties of NaPdPS<sub>4</sub>, RbPdPS<sub>4</sub>, and RbPdPS<sub>4</sub>{Rb<sub>0.33</sub>P<sub>0.4</sub>S<sub>2.23</sub>O<sub>x</sub>} are described. NaPdPS<sub>4</sub>, RbPdPS<sub>4</sub>, are isostructural and crystallize in the tetragonal system *I4/mcm* with cell parameters  $a = 7.3074(8)$  Å,  $c = 12.2308(14)$  Å and  $a = 8.2954(3)$  Å,  $c = 12.2284(4)$  Å respectively. RbPdPS<sub>4</sub>{Rb<sub>0.33</sub>P<sub>0.4</sub>S<sub>2.23</sub>O<sub>x</sub>} is cubic, space group *Pm-3n* and  $a = 12.0042(2)$  Å. All compounds contain the same  $\frac{1}{\infty}[\text{PdPS}_4]^-$  chains made of alternating square planar Pd<sup>2+</sup> cations and tetrahedral [PS<sub>4</sub>]<sup>3-</sup> anions. RbPdPS<sub>4</sub>{Rb<sub>0.33</sub>P<sub>0.4</sub>S<sub>2.23</sub>O<sub>x</sub>} contains co-crystallized highly disordered molecular species encapsulated within [Rb<sub>8</sub>] cubic cavities. Spectroscopic solid state <sup>31</sup>P NMR, infrared and Raman data as well as elemental analysis suggest that these species could be S<sub>n</sub><sup>2-</sup> ( $n = 3$  or 4) anions and possibly cationic [P<sub>4</sub>S<sub>6</sub>O]<sup>6+</sup> fragments. NaPdPS<sub>4</sub> and RbPdPS<sub>4</sub> exhibit exfoliative dissolution in polar solvents giving rise to solutions that show signs of complex fluid behavior.

© 2003 Elsevier Inc. All rights reserved.

**Keywords:** Chain-like materials; Thiophosphates; Palladium; X-ray diffraction; <sup>31</sup>P NMR; IR and Raman spectroscopies; Complex fluid; Exfoliation

## 1. Introduction

The use of thiophosphate and selenophosphate anions as ligands for the assembly of new molecular and extended structures has exposed a fascinating and astoundingly rich chemistry. This chemistry derives from the ability of these anions to engage in different ligation modes, according to the nature of the metal, its coordination preference and the metal/ligand ratio [1–3]. The major anions, in terms of frequent occurrence, are [PQ<sub>4</sub>]<sup>3-</sup> and [P<sub>2</sub>Q<sub>6</sub>]<sup>4-</sup>. They exhibit strong binding affinity for almost all elements giving rise to a large class of materials called the chalcophosphates. Other types of anions also exist but they are less studied [4]. It

is worth noting, that it is easier to attempt to access these compounds via solid state routes (e.g., direct combination or flux chemistry) rather than by solution room temperature chemistry.<sup>1</sup> Since the introduction of the polychalcophosphate flux technique in the past decade, the chemistry of the chalcophosphate class of compounds has seen a revival with an extensive variety of new structure types and materials discovered [5]. In general, these systems have been ternary and quaternary containing transition and main group metals, *M*, as well as alkali metals, *A*. They are characterized by highly anisotropic, low-dimensional structures because of the ionic character of the *A*⋯*Q* bonds and the mainly covalent character of the bonds between *M* and *Q*

\*Corresponding author. Fax: +517-353-1793.

E-mail addresses: [jobic@cnrs-irn.fr](mailto:jobic@cnrs-irn.fr) (S. Jobic), [Kanatzidis@cem.msu.edu](mailto:Kanatzidis@cem.msu.edu) (M.G. Kanatzidis).

<sup>1</sup>Undoubtedly, it is more demanding to stabilize the highly charged [P<sub>2</sub>Q<sub>6</sub>]<sup>n-</sup> species in solution and it is still more difficult to obtain corresponding crystalline products from solution.

atoms. The dimensionality of the  $M/[P_yQ_z]^{n-}$  framework is dictated by the alkali metal content, alkali metal size, and  $M/[P_yQ_z]$  ratio. In addition, we observe interesting phenomena such as dissolution in polar solvents and ion-exchange of the alkali ions with large organic cations with certain low-dimensional types of compounds such as  $\text{NaCrP}_2\text{S}_6$  [6],  $\text{NaV}_{1-x}\text{P}_2\text{S}_6$  [7],  $\text{KNiPS}_4$  [8] and  $\text{KPdPS}_4$  [9]. The ion-exchange can be either topotactic or it can induce structural rearrangements leading to molecular complexes [10].

In prior work we examined the reactivity of Pd in polychalcophosphate fluxes and we reported the synthesis, structure, and the optical and thermal properties of  $\text{K}_4\text{Pd}(\text{PS}_4)_2$ ,  $\text{Cs}_4\text{Pd}(\text{PSe}_4)_2$ ,  $\text{Cs}_{10}\text{Pd}(\text{PSe}_4)_4$ ,  $\text{KPdPS}_4$ ,  $\text{K}_2\text{PdP}_2\text{S}_6$  and  $\text{Cs}_2\text{PdP}_2\text{Se}_6$  [9]. The first three contain discrete  $[\text{Pd}(\text{PQ}_4)_2]^{4-}$  ( $Q = \text{S}, \text{Se}$ ) complexes while the latter three contain infinite one-dimensional anions. We have since extended this work to include  $\text{NaPdPS}_4$ ,  $\text{RbPdPS}_4$ , and  $\text{RbPdPS}_4\{\text{Rb}_{0.33}\text{P}_{0.4}\text{S}_{2.23}\text{O}_x\}$  and here we present and discuss these results. Remarkably, we find that while  $\text{NaPdPS}_4$ ,  $\text{RbPdPS}_4$  are isostructural to each other they are not isostructural to  $\text{KPdPS}_4$ . Equally surprising is the discovery of  $\text{RbPdPS}_4\{\text{Rb}_{0.33}\text{P}_{0.4}\text{S}_{2.23}\text{O}_x\}$  a cubic compound with infinite  $[\text{PdPS}_4]^-$  chains and co-crystallized but highly disordered  $\text{S}_3^{2-}$  anions and  $[\text{P}_4\text{S}_6\text{O}]^{6+}$  cations. We also report a rather rare property for solid state inorganic compounds (but increasingly interesting), namely the exfoliative dissolution of  $\text{NaPdPS}_4$  and  $\text{RbPdPS}_4$  in polar organic solvents to give solutions of chalcogenido macromolecules. Such solutions can in principle exhibit unique phenomena associated with complex fluid [10] and liquid crystalline behavior [11], which when deriving from purely inorganic molecules is an exceptional property.

## 2. Experimental section

### 2.1. Synthesis

All manipulations of starting materials were performed under an atmosphere of nitrogen. Starting materials were  $\text{Na}_2\text{S}$  or  $\text{Rb}_2\text{S}$ , prepared from a stoichiometric amount of elemental material sodium or rubidium and sulfur in liquid ammonia, Pd (Strem),  $\text{P}_4\text{S}_{10}$  (Aldrich, 99%) and S (99.999%, Fluka).

**NaPdPS<sub>4</sub> (I):** A mixture of 61.6 mg (0.8 mmol) of  $\text{Na}_2\text{S}$ , 140.3 mg (1.3 mmol) of Pd, 198.2 mg (0.9 mmol) of  $\text{P}_2\text{S}_5$  and 99.9 mg (3.1 mmol) of S were mixed and sealed under vacuum ( $<10^{-2}$  bar) in a silica tube. The reaction mixture was heated up to 800°C at 6°C/h, maintained at this temperature during 168 h and cool down to room temperature at 5°C/h. The reaction product contained in large amount orange needles of  $\text{NaPdPS}_4$ . Energy-dispersive X-ray spectroscopy

(EDXS) analysis of several crystals by means of a JEOL microscopy (PGT-IMIX-PTS equipped JEOL JSM5800LV) confirmed the phase composition  $\text{Na}_{1.1}\text{Pd}_{1.0}\text{P}_{1.0}\text{S}_{4.2}$ . These needles, which are the majority phase, are air stable (for weeks) and soluble in ethanol, dimethylformamide (DMF) and *N*-methylformamide (NMF). The preparation contained also red crystals of  $\text{Pd}_3(\text{PS}_4)_2$  and black crystals of PdS as minor phases.

**RbPdPS<sub>4</sub> (II):** The same procedure as in **I** was used with an amount of 267.7 mg (1.3 mmol) of  $\text{Rb}_2\text{S}$ , 234.3 mg (2.2 mmol) of Pd, 331.1 mg (1.5 mmol) of  $\text{P}_2\text{S}_5$  and 166.8 mg (5.2 mmol) of S. The product was a mixture containing orange needles of  $\text{RbPdPS}_4$  (major), and red crystals of  $\text{RbPdPS}_4\{\text{Rb}_{0.33}\text{P}_{0.4}\text{S}_{2.23}\text{O}_x\}$  (minor) and black crystals of PdS (minor) as identified by EDXS analysis. The average compositions were  $\text{Rb}_{0.9}\text{Pd}_1\text{P}_1\text{S}_{4.3}$  and  $\text{Rb}_{1.2}\text{Pd}_{1.0}\text{P}_{1.4}\text{S}_{6.8}$ , respectively. The orange needles of  $\text{RbPdPS}_4$  are air stable, slightly soluble in DMF and very soluble in NMF.

**RbPdPS<sub>4</sub>{Rb<sub>0.33</sub>P<sub>0.4</sub>S<sub>2.23</sub>O<sub>x</sub>} (III):** A mixture of Pd (0.3 mmol),  $\text{P}_2\text{S}_5$  (0.3 mmol) and  $\text{Rb}_2\text{S}_4$  (0.4 mmol) was sealed under vacuum in a silica tube and slowly heated (5°C/h) to 650°C for 10 d followed by cooling to room temperature at 10°C/h. The excess flux was removed with DMF to reveal orange, air-stable crystals (70% yield based on Pd). Microprobe analysis with a scanning electron microscope (SEM) gave an average composition of “ $\text{Rb}_{1.2}\text{PdP}_{1.4}\text{S}_{6.7}$ ”.

#### 2.1.1. Spectroscopy

Infrared spectra, in the far-IR region (650–50  $\text{cm}^{-1}$ ), were recorded at room temperature with a Nicolet 20 SF FTIR spectrometer, using a transmission technique (polyethylene pellets). The spectral resolution was 4  $\text{cm}^{-1}$  for all experiments and the spectra were corrected from substrate absorption.

The Raman scattering spectra were measured with a 1064 nm excitation from a near-infrared laser excitation (Nd:YAG laser) on a Fourier transform Raman spectrophotometer (RFS 100 Bruker). Both fine ground powder and single crystal samples were used for **(III)**, and crystals for  $\text{RbPdPS}_4$ .

The  $^{31}\text{P}$  liquid state NMR spectra were recorded on an AC 200 Bruker spectrometer, with phosphoric acid as reference ( $\delta = 0$  ppm). The  $^{31}\text{P}$  solid state NMR were recorded on a DSX400 Bruker, 9.4T, CP-MAS  $\{^1\text{H}\}$ - $^{31}\text{P}$ . Contact time 1.5 ms every 10 s. Simulation of the spectra with the software “dmfit”.

#### 2.2. Single crystal X-ray crystallography

Single crystals of **I**, **II**, and **III** were isolated from the as-prepared samples and mounted at the tip of Lindemann capillaries by means of silicone glue. All structures were solved with direct methods using

Table 1  
Crystal, X-ray data collection and refinement parameters for NaPdPS<sub>4</sub>, RbPdPS<sub>4</sub> and RbPdPS<sub>4</sub>{Rb<sub>0.33</sub>P<sub>0.4</sub>S<sub>2.23</sub>O<sub>x</sub>}<sup>b</sup>

Compound	I	II	III
Chemical formula	NaPdPS <sub>4</sub>	RbPdPS <sub>4</sub>	RbPdPS <sub>4</sub> {Rb <sub>0.33</sub> P <sub>0.4</sub> S <sub>2.23</sub> O <sub>x</sub> } <sup>b</sup>
Molecular weight (g.mol <sup>-1</sup> )	288.61	351.08	> 379.6 <sup>b</sup>
Density (g.cm <sup>-3</sup> ), calc	2.934	2.774	> 2.19 <sup>b</sup>
Crystal system	Tetragonal		Cubic
Space group	<i>I4/mcm</i>		<i>Pm-3n</i>
Cell parameters			
<i>a</i> (Å)	7.3074(8)	8.2954(3)	12.0042(2)
<i>c</i> (Å)	12.2308(14)	12.2284(4)	
<i>V</i> (Å <sup>3</sup> )	653.10(13)	841.48(5)	1729.85(4)
<i>Z</i>	4	4	6
No. of refl. for cell param.	3433	613	2939
Color	Yellow–orange	Yellow–orange	Red
Diffractometer	Stoe IPDS	Bruker–Nonius KappaCCD	
Temperature		298 K	
Radiation		MoK-L <sub>2,3</sub> (0.71069 Å)	
Monochromator		Oriented graphite (002)	
Scan mode		$\omega$	$\varphi\&\omega$
Sin( $\theta$ )/ $\lambda$ range (Å <sup>-1</sup> )	0–0.65	0–0.8	0–0.8
	$-9 \leq h \leq 9$	$-13 \leq h \leq 13$	$-16 \leq h \leq 19$
<i>hkl</i> range	$-9 \leq k \leq 9$	$-12 \leq k \leq 13$	$-17 \leq k \leq 19$
	$-14 \leq l \leq 14$	$-18 \leq l \leq 19$	$-18 \leq l \leq 18$
Number of reflections	2900	6979	12129
No. of observed reflections	2237	4928	8806
Criterion for observed reflections		$I > 2\sigma(I)$	$I > 3\sigma(I)$
No. of independent reflections	215	517	684
Crystal description	Needle	Needle	Prism
Crystal dimension (mm <sup>3</sup> )	0.1 × 0.15 × 4.0	0.06 × 0.06 × 0.4	0.2 × 0.2 × 0.2
Absorption coeff (mm <sup>-1</sup> )	4.296	8.945	> 7.99 <sup>b</sup>
$R_{\text{int(obs/all)}}$	0.075/0.076	0.143/0.147	0.067/0.101
Refinement		$F^2$	
$F(000)$	544	648	> 1046 <sup>b</sup>
Reflections used in refinement (all)	215	517	684
Reflections used in refinement (obs)	189	367	339
Refined parameters	15	17	19
$R_{\text{(obs)}/R_{\text{w(obs)}}$ <sup>a</sup>	0.0198/0.0461	0.0425/0.1223	0.0549/0.152
$R_{\text{(all)}/R_{\text{w(all)}}$ <sup>a</sup>	0.0222/0.0465	0.0713/0.1441	0.131/0.164
Weighting scheme		$w_{F^2} = 1/(\sigma^2(I_0) + 0.016 \times I_0^2)$	$w_{F^2} = 1/(\sigma^2(I_0) + 0.022 \times I_0^2)$
Diff. Fourier residues (e <sup>-</sup> /Å <sup>3</sup> )	[-0.64; 0.67]	[-1.09; 2.12]	[-0.86; 1.16]
Extinction coeff.	0.043(8)	—	—

$$^a R = \sum ||F_o| - |F_c|| / \sum |F_o|; wR_{F^2} = [\sum w(F_o^2 - F_c^2)^2 / \sum wF_o^4]^{1/2}.$$

<sup>b</sup>In the structure refinement, the Rb<sub>1.33</sub>PdPS<sub>4</sub> formulae were taken into account (see text).

SHELXS [12] and all subsequent calculations were carried out with JANA2000 [13].

**NaPdPS<sub>4</sub> and RbPdPS<sub>4</sub>.** Reflection intensities of **I** were collected at room temperature on a Stoe imaging plate diffraction system (IPDS), which was configured with IP at 60 mm limiting sin( $\theta$ )/ $\lambda$  values to 0.65 Å<sup>-1</sup>. 3433 Bragg reflections were used for cell determination and cell parameter refinement (tetragonal lattice, see Table 1). Reflection intensities of **II** were collected at room temperature on a Bruker–Nonius KappaCCD X-ray diffractometer. After the intensity integration in a tetragonal system, the cell parameters were determined from 613 reflections (see Table 1). After the usual Lorentz adjustment, the set of reflections of **I** and **II**

were analytically corrected for absorption (Gaussian integration method).

For **I**, the redundant set of 2900 reflections was then merged according to the *4/mmm* point group, yielding  $R_{\text{int(obs/all)}} = 0.075/0.076$  (215 independent reflections, of which 189 observed at a  $2\sigma(I)$  level). Refinement using anisotropic displacement parameters quickly converged to  $R_{\text{(obs)}/wR_{F^2}} = 0.0198/0.0461$  (15 parameters).

For **II**, the highly redundant set of 6979 initial reflections were merged with  $R_{\text{int(obs/all)}} = 0.143/0.147$  (517 independent reflections, of which 367 observed at a  $2\sigma(I)$  level). Refinement using anisotropic displacement parameters quickly converged. However, because of the

high residue of  $5.9 e^{-} \text{Å}^{-3}$  at (0,0,0) and the important equivalent isotropic displacement parameters ( $U_{\text{eq}}$ ) of Rb1 ( $U_{\text{eq}} = 0.041 \text{Å}^2$ ), a second rubidium atom has been introduced in (0,0,0). With an occupation ratio refined to 92.5(3)%,  $U_{\text{eq}}$  of Rb1 was improved to  $0.0371(4) \text{Å}^2$  and the  $R$  factor converged slightly to  $R_{(\text{obs})}/wR_{F^2} = 0.0425/0.1223$  with 17 parameters.

**Cubic RbPdPS<sub>4</sub>{Rb<sub>0.33</sub>P<sub>0.4</sub>S<sub>2.23</sub>O<sub>x</sub>}**. Reflection intensities of **III** were collected at room temperature on a Bruker–Nonius KappaCCD X-ray diffractometer. After the intensity integration in a cubic system, the cell parameters were determined from 2939 reflections (see Table 1). After the usual Lorentz adjustment, the set of reflections of **I** and **II** were analytically corrected for absorption (Gaussian integration method). The highly redundant set of 12129 reflections were merged according to the  $m-3m$  point group with  $R_{\text{int}(\text{obs}/\text{all})} = 0.067/0.101$  (684 independent reflections, of which 339 observed at a  $3\sigma(I)$  level). Systematic extinction suggested  $Pm-3n$  or  $P-43n$  as possible space groups. Refinement in the  $Pm-3n$  centrosymmetric space group and using isotropic displacement parameters converged to the rather high residual values  $R_{(\text{obs})}/wR_{F^2} = 0.36/0.66$ . Shifting to anisotropic displacement parameters considerably improved the results with  $R_{(\text{obs})}/wR_{F^2} = 0.0847/0.217$ , indicating a high degree of disorder. Analysis of the  $U^{ij}$  values of the atoms constituting the [PdPS<sub>4</sub>] chain revealed important lateral, out of the axis displacements. The  $U^{ij}$  values of Rb suggested an even stronger disorder for that atom. At that stage, the important positive and negative residues still observed in the difference Fourier synthesis around Rb could be suppressed either by splitting the atom (i.e., moving it out of the symmetry elements) or by using Gram–Charlier development of the Debye–Waller factor. The latter solution was used since it led to lower correlation coefficients. With up to fourth order tensors for Rb, the refinement smoothly converged to the residual values  $R_{(\text{obs})}/wR_{F^2} = 0.0549/0.152$ . The disorder of Rb was then partially resolved with two maximums in the probability density function at ca (0.2217,0.2217,0.2217) and (0.2783,0.2783,0.2783). Looking at the structure, it was found that a large cubic cavity defined by the Rb atoms was empty. The residues observed for that cavity in the final difference Fourier synthesis did not show peaks significantly higher (or lower) than those observed for the rest of the cell (max at  $1.16 e^{-}/\text{Å}^3$  and min at  $-0.86 e^{-}/\text{Å}^3$ ). Attempts to fill that cavity with atoms always led to a slight improvement of the residual  $R$ -values, but with a homogeneous spread of the electron density that could not be interpreted as well-defined atoms. Notice that, basically, any position (with fractional occupancy) and any atom type could be used to fill the cavity. It was then obvious that the cavity was probably filled by a group of atoms (vide infra) but that the single crystal

X-ray diffraction analysis could not locate those atoms. Many attempts on different crystals, at room or at lower temperatures, and in different space groups, using twinning, confirmed those observations. Here, we report the structure determination for the crystal that gave the best results (larger all/obs ratio).

Crystallographic data, refinement details and related results for **I**, **II** and **III** are summarized in the Table 1. Atomic coordinates, atomic displacement parameters, and main distances and angles are given in Tables 2, 3, and 4.

### 2.3. Computational details

The calculation method used in the present work is the projector augmented wave (PAW) method [14,15] as implemented in the Vienna ab-initio simulation package (VASP) program [16]. This electronic structure method based on the density functional theory [17,18] (DFT) is an all-electron method working directly on the full valence and core wave functions, allowing an exact description of the wave function inside the augmentation region. All calculations were performed using the generalized-gradient approximation as proposed by Perdew and Wang [19]. Numerical integrations in the Brillouin zone were carried out by the tetrahedron method [20,21] on a set of 18 special  $k$ -points determined by the Monkhorst–Pack scheme [22]. Calculations were carried out on two forms of RbPdPS<sub>4</sub>, one with Rb atoms on  $4a$  sites, the other with Rb atoms on  $4c$  sites. In addition, the stability of the hypothetical NaPdPS<sub>4</sub> form of KPdPS<sub>4</sub> compared to the observed form was probed. In all the calculations, the cell parameters and the atomic positions were first optimized. Then, the total energy was calculated.

Table 2  
Fractional atomic coordinates, equivalent isotropic displacement parameters ( $\text{Å}^2$ ), occupation ratios and s.u.'s for **I**, **II** and **III**

Atoms	$x$	$y$	$z$	$U_{\text{eq}}$	$\tau$
<b>I</b>					
Na	0	0	0.25	0.0407(12)	
Pd	0.5	0	0	0.01285(16)	
P	0.5	0	0.25	0.0137(4)	
S	0.34962(8)	0.15037(8)	0.14138(8)	0.0176(2)	
<b>II</b>					
Rb1	0	0	0.25	0.0371(4)	0.925(3)
Rb2	0	0	0	0.057(6)	0.075
Pd	0.5	0	0	0.02290(19)	
P	0.5	0	0.25	0.0225(5)	
S	0.36724(10)	0.13275(10)	0.14201(9)	0.0300(3)	
<b>III</b>					
Rb	0.25	0.25	0.25	0.2490(19)	
Pd	0	0	0.5	0.0641(4)	
P	0.25	0	0.5	0.0730(10)	
S	0.14231(13)	0.13100(17)	0.5	0.0840(9)	

Table 3

Atoms	$U^{11}$	$U^{22}$	$U^{33}$	$U^{12}$	$U^{13}$	$U^{23}$
(a) $U^{ij}$ anisotropic displacement parameters ( $\text{\AA}^2$ ) and s.u.'s for <b>I</b> , <b>II</b> and <b>III</b>						
<b>I</b>						
Na	0.0291(11)	0.0291(11)	0.064(3)	0	0	0
Pd	0.0166(2)	0.0166(2)	0.0054(3)	0.00427(19)	0	0
P	0.0173(5)	0.0173(5)	0.0065(10)	0	0	0
S	0.0220(3)	0.0220(3)	0.0089(5)	0.0081(3)	0.0007(2)	−0.0007(2)
<b>II</b>						
Rb1	0.0322(5)	0.0322(5)	0.0467(9)	0	0	0
Rb2	0.069(10)	0.069(10)	0.034(11)	0	0	0
Pd	0.0314(3)	0.0314(3)	0.0058(3)	0.0023(3)	0	0
P	0.0301(9)	0.0301(9)	0.0073(10)	0	0	0
S	0.0393(5)	0.0393(5)	0.0116(5)	0.0082(5)	0.0002(3)	−0.0002(3)
<b>III</b>						
Rb	0.249(3)	0.249(3)	0.249(3)	0.111(4)	0.111(4)	0.111(4)
Pd	0.0236(5)	0.0935(9)	0.0752(8)	0	0	0
P	0.0259(13)	0.0966(18)	0.0966(18)	0	0	0
S	0.0337(8)	0.0902(14)	0.128(2)	−0.0005(9)	0	0
(b) $C^{ijk}$ and $D^{ijkl}$ Gram–Charlier non-harmonic Debye–Waller parameters <sup>a</sup> and s.u.'s for <b>III</b>						
	$C^{111}$	$C^{112}$	$C^{113}$	$C^{122}$	$C^{123}$	
Rb	0	0.0002(3)	−0.0002(3)	−0.0002(3)	0	
	$C^{133}$	$C^{222}$	$C^{223}$	$C^{233}$	$C^{333}$	
Rb	0.0002(3)	0	0.0002(3)	−0.0002(3)	0	
	$D^{1111}$	$D^{1112}$	$D^{1113}$	$D^{1122}$	$D^{1123}$	
Rb	−0.0392(17)	−0.0385(14)	−0.0385(14)	−0.0341(16)	−0.0358(18)	
	$D^{1133}$	$D^{1222}$	$D^{1223}$	$D^{1233}$	$D^{1333}$	
Rb	−0.0341(16)	−0.0385(14)	−0.0358(18)	−0.0358(18)	−0.0385(14)	
	$D^{2222}$	$D^{2223}$	$D^{2233}$	$D^{2333}$	$D^{3333}$	
Rb	−0.0392(17)	−0.0385(14)	−0.0341(16)	−0.0385(14)	−0.0392(17)	

<sup>a</sup>  $C^{ijk}$  coefficient are multiplied by  $10^3$ ;  $D^{ijkl}$  coefficient are multiplied by  $10^4$ .

Table 4

Main distances ( $\text{\AA}$ ), angles ( $^\circ$ ), and s.u.'s in **I**, **II**, and **III**

<b>I</b>	<b>II</b>	<b>III</b>
Pd–S = 2.3248(8)	Pd–S = 2.3326(9)	Pd–S = 2.3218(19)
P–S = 2.0445(8)	P–S = 2.0419(9)	P–S = 2.036(2)
S–P–S = 98.94(3)	S–P–S = 99.41(4)	S–P–S = 101.15(7)
S–P–S = 114.98(3)	S–P–S = 114.73(3)	S–P–S = 113.79(4)
S–Pd–S = 83.89(3)	S–Pd–S = 83.78(3)	S–Pd–S = 85.26(7)
S–Pd–S = 96.11(3)	S–Pd–S = 96.22(3)	S–Pd–S = 94.74(7)
Na–S = 3.0822(7)	Rb1–S = 3.4982(8)	
	Rb2–S = 3.6755(9)	

### 3. Results and discussion

#### 3.1. Description of structures

**NaPdPS<sub>4</sub>** and **RbPdPS<sub>4</sub>**. The two compounds are isostructural and adopt the space group  $I4/mcm$ . The

tetragonal organization of the chains, which are parallel to one another and run along the 4-fold rotation axis, is shown in Fig. 1. Both contain the same one-dimensional polymeric  $\frac{1}{\infty}[\text{PdPS}_4]^-$  chains of alternating square planar  $\text{Pd}^{2+}$  atoms and tetrahedral  $[\text{PS}_4]^{3-}$  anions. The Pd–S distances are 2.3248(8)  $\text{\AA}$  and 2.3326(9)  $\text{\AA}$  for the Na and Rb analogs, respectively.

The alkali metal atoms are arranged in straight lines along the *c*-axis and are situated in square antiprismatic 8-coordinate sites (4*a* Wyckoff symbol) with Na–S and Rb–S bonds of 3.0822(7)  $\text{\AA}$  and 3.4982(8)  $\text{\AA}$  respectively. Although normal for  $\text{Rb}^+$  this is an exceptionally high coordination number for  $\text{Na}^+$  which generally prefers a lower number. This highly symmetric cage for the alkali metal atoms is in sharp contrast with the decidedly irregular cage of  $\text{K}^+$  ions in  $\text{KPdPS}_4$ . Interestingly, along the rows of alkali ions exists a second vacant 8-coordinate site (4*c* Wyckoff symbol), which has a compressed square prismatic (cubic) geometry. A small degree of occupation of this site in the case of  $\text{RbPdPS}_4$

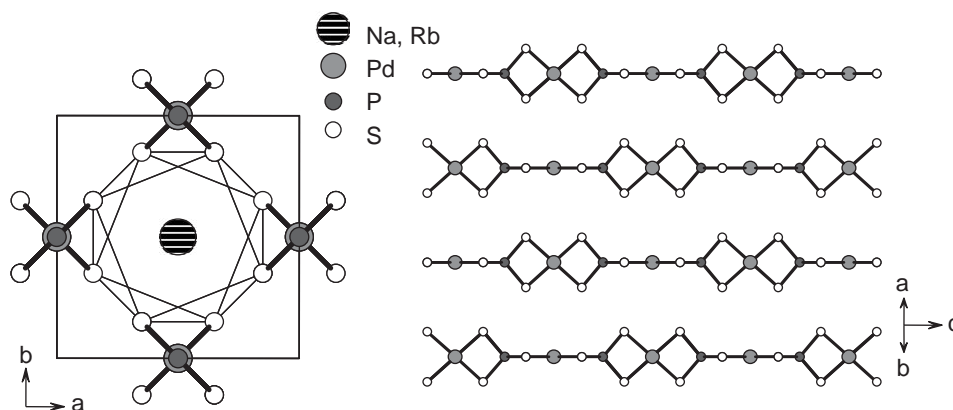


Fig. 1. The structure NaPdPS<sub>4</sub> and RbPdPS<sub>4</sub> (A) viewed down the *c*-axis with the representation of the antiprismatic polyhedra, (B) viewed down the [110] direction of one layer of  $\frac{1}{2}$ [PdPS<sub>4</sub>]<sup>−</sup> chains.

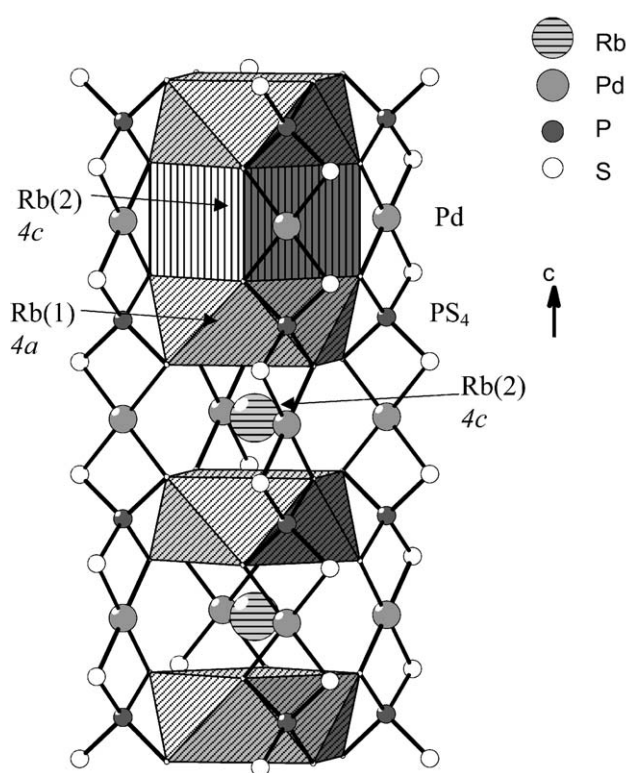


Fig. 2. A section of the crystal structure of NaPdPS<sub>4</sub> and RbPdPS<sub>4</sub> showing the square-antiprismatic and square-prismatic shape of the alkali metal cavities. The 4*a*-site is surrounded by tetrahedral [PS<sub>4</sub>]<sup>3−</sup> anions while the 4*c* site is surrounded by square planar [PdS<sub>4</sub>]<sup>6−</sup> anions. In the Na analog the latter site is vacant.

gives rise to the only structural difference that exists between NaPdPS<sub>4</sub> and RbPdPS<sub>4</sub>. Apparently, 7.5(3)% of the Rb atoms “spill over” into this site whereas this does not occur with Na. Electronic calculations carried out on RbPdPS<sub>4</sub> with Rb atoms either on 4*a* sites or 4*c* sites confirms the higher stability of the 4*a* site compared to the 4*c* site ( $\Delta E = 126$  meV/unit formulae). A close inspection of the crystal structure reveals that the 4*a* site

is adjacent to the negatively charged [PS<sub>4</sub>]<sup>3−</sup> anions and thus a greater electrostatic stabilization is achieved with the alkali metal atoms in it, Fig. 2. In contrast the 4*c* position lies closer to the positively charged Pd<sup>2+</sup> centers. The slight occupation of this site in the case of Rb<sup>+</sup> but not Na<sup>+</sup> is probably due to the more diffuse nature of positive charge in the former. The overall organization and space group symmetry is the same as many other chain type compounds such as TlSe [23], NaInTe<sub>2</sub> [24], K<sub>2</sub>HgSnTe<sub>4</sub> [25], etc., however these phases have formally one additional alkali metal cation in the structure.

The structure of the [PdPS<sub>4</sub>]<sup>−</sup> anion, remains the same as we move from Na to K to Rb and therefore there is an absence of a counterion effect [26]. This is consistent with the high stability of these chains recognized in earlier studies in solution [10]. The significant difference, however, between the APdPS<sub>4</sub> (*A* = Na and Rb) and KPdPS<sub>4</sub> structure types is the arrangement of the chains within the unit cell. In KPdPS<sub>4</sub> (isomorphous to KNiPS<sub>4</sub>) the chains, perpendicular to the 4-fold rotation axis of the tetragonal cell, run in a parallel fashion successively along the [110] and [−110] directions, see Fig. 3, whereas in the Na and Rb analogs, the chains are all parallel to the [001] axis. It is peculiar that the Na and Rb salts are isostructural but the K salt, lying in the middle of the series is not. Instead this material adopts a different packing arrangement and space group (*P4*<sub>2</sub>/*mmm*). It is thus inevitable to predict that a second form of KPdPS<sub>4</sub> (e.g.,  $\beta$ -phase) should also be stable but has not been yet identified.

To gain some insight into the exceptional behavior of the K salt, we performed electronic structure calculations and examined the relative stability of the two forms of this composition (i.e., the observed KNiPS<sub>4</sub>-type and the hypothetical NaPdPS<sub>4</sub>-type of KPdPS<sub>4</sub>, hereafter named  $\alpha$ -KPdPS<sub>4</sub> and  $\beta$ -KPdPS<sub>4</sub>, respectively). As crystal data were reproduced with less than 2% difference for  $\alpha$ -KPdPS<sub>4</sub>, optimization of the cell parameters and the atom positions of  $\beta$ -KPdPS<sub>4</sub> is

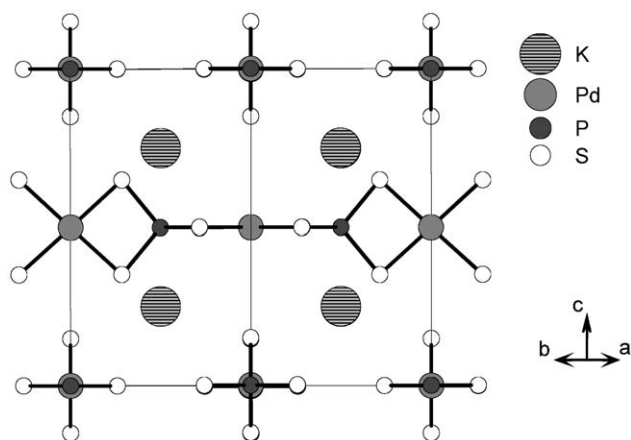


Fig. 3. Structure of  $\text{KPdPS}_4$  viewed down the  $[110]$  axis showing the mutually perpendicular chains of  $[\text{PdPS}_4]^-$  in two successive  $\frac{1}{\infty}[\text{PdPS}_4]^-$  layers.

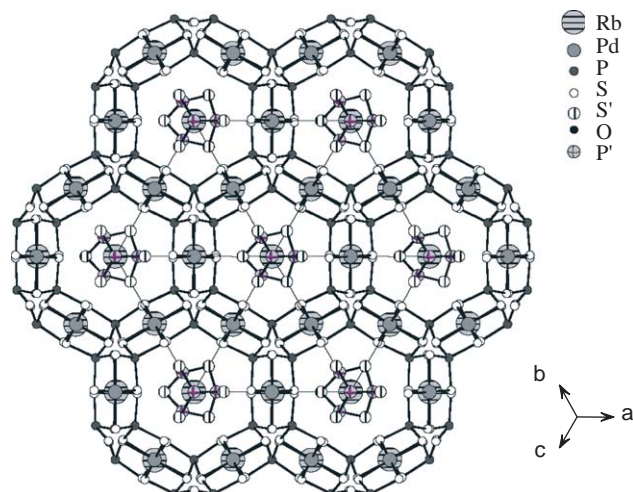


Fig. 5. Structure of **III** viewed down the  $[111]$  direction, showing the large parallel tunnels present. These tunnels host the co-crystallized  $\{\text{Rb}_{0.33}\text{P}_{0.4}\text{S}_{2.23}\text{O}_x\}$  material.

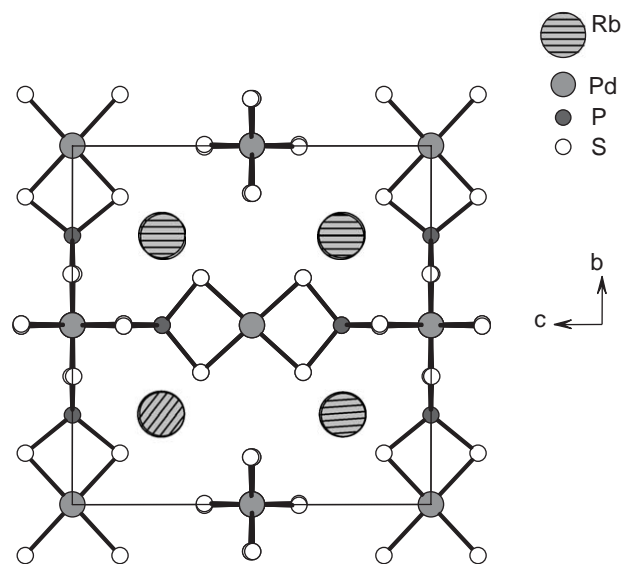


Fig. 4. Structure of **III** viewed down the  $[100]$ . The co-crystallized fragments have been removed for clarity.

trustworthy. In both cases, calculations lead to indistinguishable  $\frac{1}{\infty}[\text{PdPS}_4]$  chains with very similar Pd–S and P–S distances (2.353 and 2.364 Å against 2.358 Å for Pd–S contacts and 2.055 and 2.064 Å against 2.066 Å for P–S contacts in  $\alpha$ - $\text{KPdPS}_4$  and  $\beta$ - $\text{KPdPS}_4$ , respectively) with a unit volume per formula unit lower for the  $\beta$ -form by  $4.59 \text{ \AA}^3$ . As the calculated total energy difference between the two forms ( $\Delta E = 4 \text{ meV/formulae unit}$ ) is insignificant and within the uncertainty of the calculation method, the stabilization of  $\beta$ - $\text{KPdPS}_4$  might be possible in “out-of-equilibrium” conditions or under high pressure, in a diamond anvil cell for instance.

**The cubic  $\text{RbPdPS}_4\{\text{Rb}_{0.33}\text{P}_{0.4}\text{S}_{2.23}\text{O}_x\}$ .** This compound is somewhat curious in that it is a co-crystallate

of  $\text{RbPdPS}_4$  and two additional species, one of them unique. The structure is highly symmetric described by the cubic space group  $Pm-3n$ . It contains the same  $[\text{PdPS}_4]^-$  chains as all  $\text{APdPS}_4$  phases but the cubic symmetry enforces a mutually perpendicular orientation of three chains along the unit cell axes, see Fig. 4. A similar arrangement of the  $\frac{1}{\infty}[\text{PdPS}_4]^-$  chains is present in  $\text{KPdPS}_4$  (see Fig. 3) but it involves only two chains consistent with the tetragonal geometry. When the chains pack in the fashion found in  $\text{RbPdPS}_4\{\text{Rb}_{0.33}\text{P}_{0.4}\text{S}_{2.23}\text{O}_x\}$  they leave void space in the form of large tunnels running along the body diagonal of the cubic cell, i.e.,  $[111]$  direction, Fig. 5. These tunnels contain the Rb atoms but they are too large for these having a diameter of  $\sim 6 \text{ \AA}$ , and evidently are filled with other species. To accommodate these extra matter the average chain–chain distance in this material is slightly larger (by  $\sim 0.16 \text{ \AA}$ ) than that observed in  $\text{RbPdPS}_4$ . The electron density in the  $[\text{Rb}_8]$  cubic cavities ( $6.02 \times 6.02 \times 6.02 \text{ \AA}^3$ ) is quite diffuse because of the high degree of disorder created by the high crystallographic symmetry of this site. The disorder is static as it did not change significantly when the refinement of the crystal structure was performed at 77 K.

At this stage let only mention that solid state  $^{31}\text{P}$  NMR of polycrystalline powder samples of  $\text{RbPdPS}_4\{\text{Rb}_{0.33}\text{P}_{0.4}\text{S}_{2.23}\text{O}_x\}$  show clearly two resonances at 145 and 43 ppm in the ratio  $\sim 75/25\%$  respectively, see Fig. 6. The first resonance at 145 ppm is assigned to the  $[\text{PS}_4]^{3-}$  unit of the  $[\text{PdPS}_4]^-$  chain (by virtue of its close similarity to that of the  $\text{RbPdPS}_4$ , presented below) whereas the second could be due to the phosphorus atoms encapsulated in the  $[\text{Rb}_8]$  cubic cavities. The single resonance at 43 ppm can only be attributed to a high point-group symmetry of a phosphorus oxysulfide species ( $[\text{P}_4\text{S}_6\text{O}]^{6+}$  for instance)

rendering all P atoms equivalent. The upfield location of the hypothetical  $[\text{P}_4\text{S}_6\text{O}]^{6+}$  group resonance relative to that of the  $[\text{PS}_4]^{3-}$  unit would be consistent with trends reported in the literature regarding P–S and P–O species [27].

Based on the only microprobe analyses of **(III)** (see above), and in comparison with those of **(II)** which correspond to the  $\text{RbPdPS}_4$  chemical composition, we can derive the approximated  $\text{Rb}_{1.333}\text{PdP}_{1.4}\text{S}_{6.23}$  formulae for **(III)**, i.e.,  $\text{RbPdPS}_4\{\text{Rb}_{0.333}\text{P}_{0.4}\text{S}_{2.23}\}$ . As aforementioned, based on  $^{31}\text{P}$  NMR measurements, this formulae has to be modified to take into account the occurrence of P–O bonds. Consequently, the right formulae might be rewritten,  $\text{RbPdPS}_4\{\text{Rb}_{0.33}\text{P}_{0.4}\text{S}_{2.23}\text{O}_x\}$ , with  $x$  undefined. As the  $\text{RbPdPS}_4$

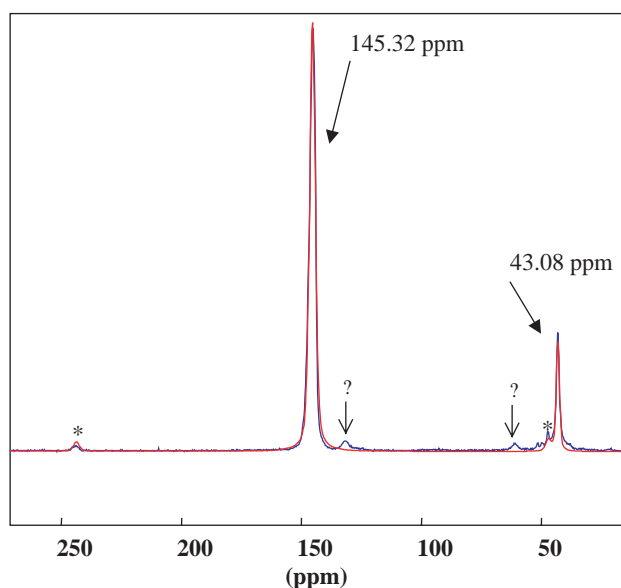


Fig. 6. Solid state  $^{31}\text{P}$  NMR spectrum CP-MAS  $\{^1\text{H}\}$ - $^{31}\text{P}$  of  $\text{RbPdPS}_4\{\text{Rb}_{0.33}\text{P}_{0.4}\text{S}_{2.23}\text{O}_x\}$ . The resonance at 145.32 ppm corresponds to the P atoms of the chains while the signal at 43.08 ppm is assigned to the  $[\text{P}_4\text{S}_6\text{O}]^{6+}$  group. Rotation bands are underlined with an asterisk.

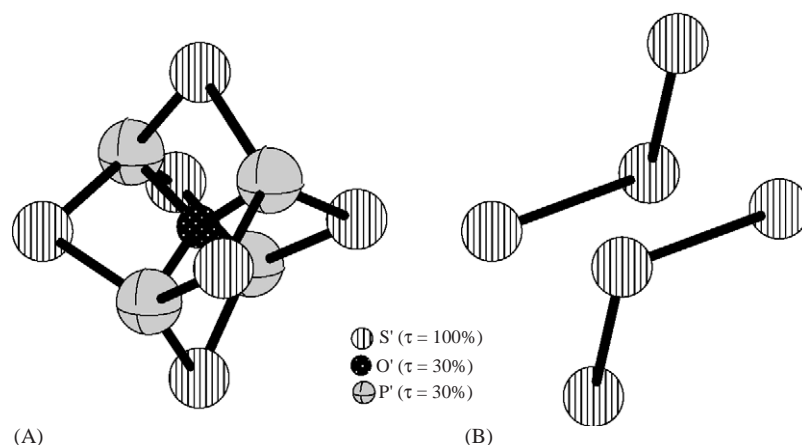


Fig. 7. The putative molecular species in  $\text{RbPdPS}_4\{\text{Rb}_{0.33}\text{P}_{0.4}\text{S}_{2.23}\text{O}_x\}$ : (A)  $[\text{P}_4\text{S}_6\text{O}]^{6+}$  and (B) a trisulfide  $\text{S}_3^{2-}$  anion.

sub-network is neutral (see **(II)**), the “ $\text{Rb}_{0.33}\text{P}_{0.4}\text{S}_{2.23}\text{O}_x$ ” species has to be too. Based on charge balance arguments, the occurrence of  $[\text{PS}_4]^{3-}$  groups, as  $[\text{P}_2\text{S}_n]^{4-}$  entities ( $n = 6, 7, 9$  for instance) can be ruled out: the charge balance may only be ensured if molecular  $[\text{P}_4\text{Q}_n]$  species ( $\text{Q} = \text{O}, \text{S}; n = 6, 7, 8, 9$  or 10) occur concomitantly with  $[\text{S}_n]^{2-}$  oligomers, or more likely, if  $[\text{PO}_x\text{S}_y]^{n+}$  cations are stabilized with  $[\text{S}_n]^{2-}$  counter-anions. Let us remind that the  $[\text{P}_4\text{Q}_n]$  neutral species and the  $[\text{PO}_x\text{S}_y]^{n+}$  cations are constrained to fit the  $[\text{Rb}_8]$  cubic cavity dimensions, i.e.,  $6.02 \times 6.02 \times 6.02 \text{ \AA}^3$ . Moreover, from vibrational spectroscopy (see below), polysulfide  $[\text{S}_3]^{2-}$  or  $[\text{S}_4]^{2-}$  fragments are suspected. Thus, this implies that the  $[\text{P}_{0.4}\text{S}_{2.23}\text{O}_x]^{0.33-}$  species can be decomposed either into  $0.165 \times [\text{S}_3]^{2-}$  and  $0.1 \times [\text{P}_4\text{S}_{17.35}\text{O}_{10x}]^0$  (unlikely entities), or into  $[\text{S}_3]^{2-}$  in higher concentration and  $[\text{PO}_x\text{S}_y]$  cationic fragments issued from the condensation of  $[\text{PQ}_4]$  tetrahedra. Such cationic species can only be obtained if more than two  $[\text{PQ}_4]$  entities condense. Consequently, as P atoms have to be equivalent, and as this new species has to fit the cubic cavities, only two cationic phosphorus oxysulfides cations could be suitable:  $[\text{P}_3\text{OS}_6]^+$  and  $[\text{P}_4\text{S}_6\text{O}]^{6+}$ . For charge balance criteria, only the last solution can be retained. Fig. 7 depicts this putative species along with the co-habiting trisulfide ions.

The origin of these species, or at least, any other phosphorus oxysulfides, is almost certainly the flux in which the material was prepared. The presence of a P–S–O species such as the proposed  $[\text{P}_4\text{S}_6\text{O}]^{6+}$  in the crystal is surprising and, given that it has not been previously observed, makes us cautious as to its accuracy. Verification of its existence must await an independent synthesis of this cation. Nevertheless, regardless of the precise structure, it is tempting to consider that its formation was caused by some sort of templating action, produced by packing the  $[\text{PdPS}_4]^-$  chains in cubic symmetry or vice versa.

### 3.2. Synthesis, spectroscopy and chemical considerations

The synthesis of NaPdPS<sub>4</sub>, and RbPdPS<sub>4</sub>, is relatively straightforward and was accomplished with direct combination reactions at 800°C as described in Section 2. The stabilization of RbPdPS<sub>4</sub>{Rb<sub>0.33</sub>P<sub>0.4</sub>S<sub>2.23</sub>O<sub>x</sub>} however, required the use of a polythiophosphate flux which evidently provided the extra material found co-crystallized in the lattice. The presence of oxygen in the compound is attributed to adventitious P–O bonded species in the flux or even moisture. RbPdPS<sub>4</sub>{Rb<sub>0.33</sub>P<sub>0.4</sub>S<sub>2.23</sub>O<sub>x</sub>} can also be prepared as a mixture with RbPdPS<sub>4</sub>, using a stoichiometric reactant ratio.

**Solubility and <sup>31</sup>P NMR studies.** A fascinating property exhibited by NaPdPS<sub>4</sub> and RbPdPS<sub>4</sub> is their facile dissolution in appropriate polar solvents, after which polymeric chalcogenide chains may persist for a limited time, giving rise to complex fluid behavior. Their dispersion/dissolution properties were studied and compared with those of KPdPS<sub>4</sub>. These three compounds disperse their chains upon interaction with polar

solvent molecules to give light orange solutions when the compound/solvent molar ratio is low, and a thick orange gel at higher concentrations.

The solubility of the three compounds was determined in different solvents: NaPdPS<sub>4</sub> was found to be soluble in acetone ( $\epsilon = 20$ ), ethanol ( $\epsilon = 25$ ), DMF ( $\epsilon = 37$ ), dimethylsulfoxide (DMSO,  $\epsilon = 46$ ) and NMF ( $\epsilon = 182$ ). KPdPS<sub>4</sub> was found to be soluble in DMF, DMSO and NMF only, whereas RbPdPS<sub>4</sub> is partly soluble in DMF but very soluble in NMF. These results show clearly the trend of increasing solubility with decreasing counteraction size and with increasing the dielectric constants of the solvent. Indeed, the smaller the alkali metal and the more polar the solvent the higher their interaction because of the higher solvation energy. Geometrically speaking, the solvation weakens greatly the electrostatic bonding interactions between the alkali ions and [PdPS<sub>4</sub>]<sup>−</sup> macro-chains allowing chain dispersal in solution. Remarkably, RbPdPS<sub>4</sub>{Rb<sub>0.33</sub>P<sub>0.4</sub>S<sub>2.23</sub>O<sub>x</sub>} did not dissolve in any solvent we tried.

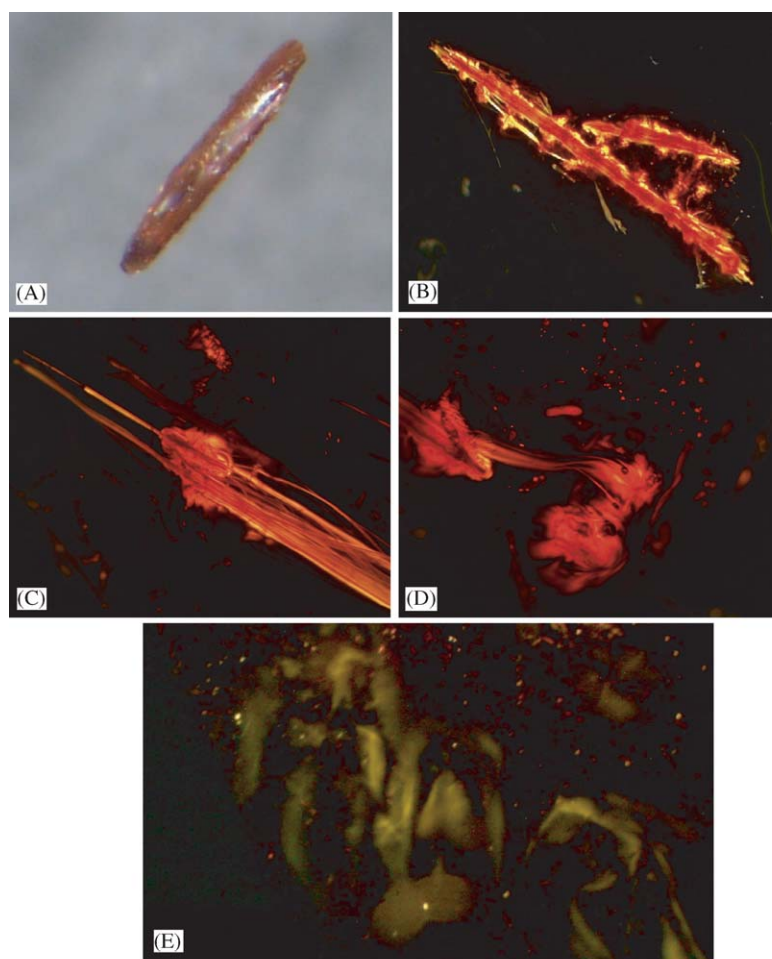


Fig. 8. Microscope photographs RbPdPS<sub>4</sub> dissolving in NMF. (A) A needle-like crystal of RbPdPS<sub>4</sub>. (B)–(D) Exfoliation process at different steps after the deposition of one drop of NMF on a crystal. (E) Transient birefringence observed under polarized light from a sheared solution of RbPdPS<sub>4</sub>/NMF.

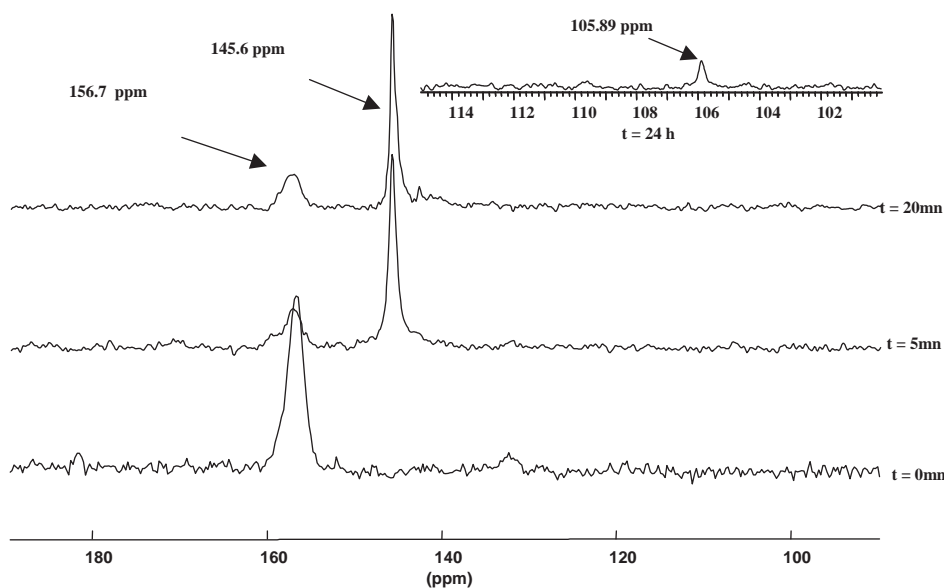


Fig. 9. Solid state  $^{31}\text{P}$  NMR spectra of RbPdPS<sub>4</sub>.  $t = 0$  min: spectrum of crystals of RbPdPS<sub>4</sub>. The resonance at 156.7 ppm corresponds to the signal of the P atoms in the chains by analogy with the signal at 149 ppm obtained for crystals of KPdPS<sub>4</sub>.  $t = 5$  min: Spectrum 5 min after one drop of NMF has been introduced in situ at room temperature leading to a gel.  $t = 20$  min: Spectrum 20 min after addition of the NMF drop showing a new resonance at 145.6 ppm.

To compare the dissolution of all three APdPS<sub>4</sub> compounds, the behavior of crystals was observed when NMF drops were added. In every case, the crystals immediately swelled upon contact with the solvent to give first a gel and then an orange solution. The process of a crystal of APdPS<sub>4</sub> dissolving in NMF is shown in different stages in Fig. 8. The birefringence, observed by optical microscopy under polarized light (crossed polarized) of the solution surrounding the crystal decreased as the distance from the crystal increased. When the crystal totally dissolved, the birefringence slowly disappeared, and within a few minutes at room temperature the solutions appeared isotropic. If the solutions were then sheared, a transient birefringence was immediately observed again. However, as the solutions of APdPS<sub>4</sub> aged, the intensity of this transient birefringence decreased to zero. The loss of transient birefringence appeared after a few minutes for Na and K phases and after  $\sim 1$  h for the Rb phase and suggests that the macro-chains are no longer intact in NMF. In contrast, infinite  $[\text{PdPS}_4]^-$  chains are stable in DMF-KPdPS<sub>4</sub> solutions with respect to time in ambient conditions and the transient birefringence can be reproduced indefinitely [10].

To shed some light on the dissolution process of APdPS<sub>4</sub> materials ( $A = \text{Na}, \text{Rb}$ ) in NMF, solid and solution  $^{31}\text{P}$  NMR experiments were performed on crystals, gels and solutions. First, some crystals of NaPdPS<sub>4</sub> and RbPdPS<sub>4</sub>, were selected and exfoliated in NMF by stirring vigorously for 2 h under nitrogen atmosphere at room temperature. A similar KPdPS<sub>4</sub> solution was prepared as reference. The concentrations

of the three orange solutions were  $1.0 \times 10^{-2}$ ,  $4.9 \times 10^{-2}$  and  $2.9 \times 10^{-2}$  mol/L for NaPdPS<sub>4</sub>, KPdPS<sub>4</sub>, RbPdPS<sub>4</sub>, respectively. All three solution state  $^{31}\text{P}$  NMR spectra, obtained  $\sim 24$  h after the preparation of the solutions, show only one signal at 105.9 ppm. By comparison, liquid state the  $^{31}\text{P}$  resonance of DMF-KPdPS<sub>4</sub> solutions is at 146.9 ppm, which is close to the peak at 149 ppm observed in the solid state  $^{31}\text{P}$  NMR spectra of KPdPS<sub>4</sub> powder [10]. To understand this 41 ppm signal shift, a study of the dissolution process at different rigid stages has been undertaken by solid state  $^{31}\text{P}$  NMR on RbPdPS<sub>4</sub> crystals and gels (Fig. 9).

Prior to adding NMF to RbPdPS<sub>4</sub> crystals, a single resonance is observed at 156.7 ppm ( $t = 0$ ). Upon addition of NMF and initiation of chain dissolution the resonance at 156.7 ppm decreases and a new one emerges at 145.6 ppm ( $t = 5$  min). This is very similar to the single resonance observed for KPdPS<sub>4</sub> at 146.4 ppm, corresponding to the signal of the chains in solution.<sup>2</sup> That these NMF solutions show shear-induced birefringence also supports the conclusion of intact chains. Upon standing for  $> 1$  h, the peak at 145.6 ppm begins to disappear and this is concomitant with the vanishing of birefringence. At this point the NMR spectrum shows only a weak resonance at 105.89 ppm ( $t = 24$  h) which

<sup>2</sup> Given the presence of birefringence of the solution, it is unlikely that the signal at 145.6 ppm could correspond to molecular oligomeric species such as the hypothetical  $[\text{Pd}_3(\text{PS}_4)_3]^{3-}$  or  $[\text{Pd}_4(\text{PS}_4)_4]^{4-}$  complexes. Nevertheless such complexes may be forming in KPdPS<sub>4</sub>/DMF solutions heated at 75°C for 23 days, according to electrospray mass spectroscopy and NMR spectroscopy which reveals two resonances at 143.3 and 142.8 ppm see Ref. [28].

could be attributed to an oxo-thiophosphate species and signifies the decomposition of the  $\frac{1}{\infty}[\text{PdPS}_4]^-$  chains or, less likely, to new  $[\text{Pd}_n\text{P}_n\text{S}_{4n}]^{-3n}$  species ( $n \geq 4$ ) [28].

Based on these data we can conclude that the  $\frac{1}{\infty}[\text{PdPS}_4]^-$  chains in all  $\text{APdPS}_4$  are intact after dispersion in NMF for a limited time. The alkali metal cations play an insignificant role in affecting the anionic covalent structure in solution. The limited hour-long stability in NMF is still impressive given the exceptionally strong polar nature of this solvent. As determined earlier for  $\text{KPdPS}_4$ , the chains are considerably more stable in DMF lasting for days [10], and this is consistent with our previous assessments that the  $\frac{1}{\infty}[\text{PdPS}_4]^-$  chains are relatively robust.

**Vibrational spectroscopy.** In order to confirm the presence of the chains  $\frac{1}{\infty}[\text{PdPS}_4]^-$  in  $\text{RbPdPS}_4$  and

$\text{RbPdPS}_4\{\text{Rb}_{0.33}\text{P}_{0.4}\text{S}_{2.23}\text{O}_x\}$  compounds and to get some insight concerning the nature of the molecular species in **III** at the beginning of our structural refinement, IR and Raman spectroscopic studies were performed on crystals of the former and ground powder of the latter.

The far-IR and Raman data were in good agreement with those observed for the  $\text{KPdPS}_4$  compound. The spectra are shown in Fig. 10 and the results are summarized in Table 5. The far-IR spectra, display two absorptions at  $553\text{--}588\text{ cm}^{-1}$  for  $\text{RbPdPS}_4$  and  $553\text{--}592\text{ cm}^{-1}$  for  $\text{RbPdPS}_4\{\text{Rb}_{0.33}\text{P}_{0.4}\text{S}_{2.23}\text{O}_x\}$  which can be assigned to  $\text{PS}_4$  asymmetric stretching modes ( $\nu_{\text{asym}}(\text{PS}_4)^{3-}$ ). The absorption at  $322\text{ cm}^{-1}$  for  $\text{RbPdPS}_4$  is mainly attributed to S–Rb–S bending modes ( $\delta(\text{SRbS})$ ) and to  $\text{PdS}_4$  asymmetric stretching modes

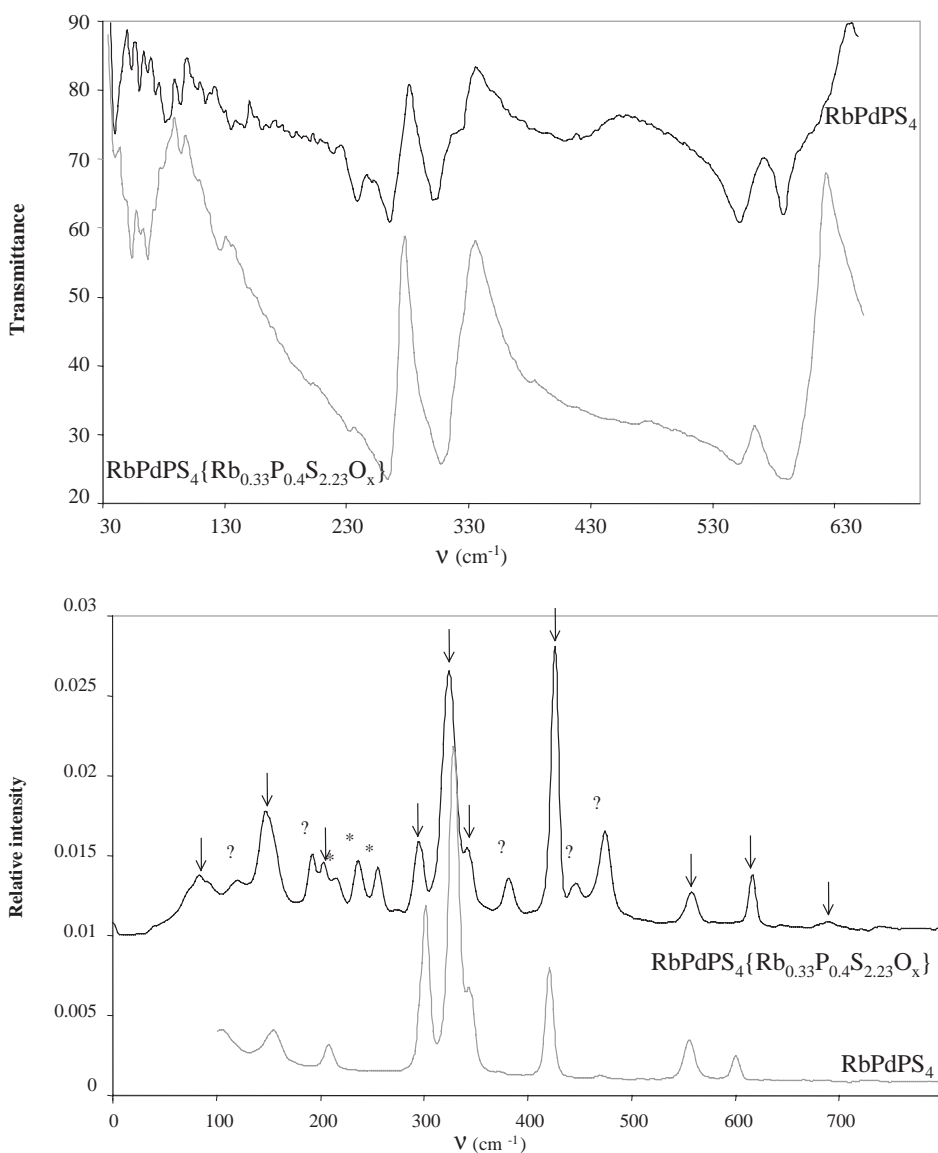


Fig. 10. Top: Infrared spectra, and bottom: Raman spectra of  $\text{RbPdPS}_4$  and  $\text{RbPdPS}_4\{\text{Rb}_{0.33}\text{P}_{0.4}\text{S}_{2.23}\text{O}_x\}$ .

( $\nu_{\text{asym}}(\text{PdS}_4)$ ), Fig. 10A. Similar assignments were made earlier in the case of  $\text{KPdPS}_4$  [29]. The peaks at  $302\text{--}239\text{ cm}^{-1}$  and  $310\text{--}233\text{ cm}^{-1}$  for  $\text{RbPdPS}_4$  and  $\text{RbPdPS}_4\{\text{Rb}_{0.33}\text{P}_{0.4}\text{S}_{2.23}\text{O}_x\}$  respectively can be attributed to  $\text{PdS}_4$  bending modes ( $\delta(\text{PdS}_4)$ ). The peak at  $266\text{ cm}^{-1}$  for  $\text{RbPdPS}_4$  and  $264\text{ cm}^{-1}$  for  $\text{RbPdPS}_4\{\text{Rb}_{0.33}\text{P}_{0.4}\text{S}_{2.23}\text{O}_x\}$  are attributed mainly to a S–Rb–S bending mode ( $\delta(\text{SRbS})$ ) and to  $\text{PS}_4$  bending modes ( $\delta(\text{PS}_4)^{3-}$ ).

The Raman spectra display bands at  $600, 556$  and  $421\text{ cm}^{-1}$  for  $\text{RbPdPS}_4$  and  $617, 560$  and  $426\text{ cm}^{-1}$  for  $\text{RbPdPS}_4\{\text{Rb}_{0.33}\text{P}_{0.4}\text{S}_{2.23}\text{O}_x\}$  which can be assigned to  $\text{PS}_4$  stretching modes ( $\nu(\text{PS}_4)^{3-}$ ). The bands at  $344\text{--}328\text{ cm}^{-1}$  for  $\text{RbPdPS}_4$  and  $343\text{--}324\text{ cm}^{-1}$  for  $\text{RbPdPS}_4\{\text{Rb}_{0.33}(\text{S}_3^{2-})_{0.46}[\text{P}_4\text{S}_6\text{O}]_{0.1}^{6+}\}$  can be assigned to  $\text{PdS}_4$  stretching modes ( $\nu(\text{PdS}_4)$ ) and those at  $209$  and  $204\text{ cm}^{-1}$ , respectively to  $\text{PdS}_4$  bending modes ( $\delta(\text{PdS}_4)$ ), Fig. 10B. Finally, the bands at  $301$  and  $157\text{ cm}^{-1}$  for  $\text{RbPdPS}_4$  and  $295$  and  $149\text{ cm}^{-1}$  for  $\text{RbPdPS}_4\{\text{Rb}_{0.33}(\text{S}_3^{2-})_{0.46}[\text{P}_4\text{S}_6\text{O}]_{0.1}^{6+}\}$  are attributed mainly to S–Rb–S bending modes ( $\delta(\text{SRbS})$ ) and to  $\text{PS}_4$  asymmetric bending modes ( $\delta_{\text{asym}}(\text{PS}_4)^{3-}$ ). The signals at  $216\text{--}237\text{ cm}^{-1}$  and  $448\text{--}475\text{ cm}^{-1}$  for  $\text{RbPdPS}_4\{\text{Rb}_{0.33}(\text{S}_3^{2-})_{0.46}[\text{P}_4\text{S}_6\text{O}]_{0.1}^{6+}\}$  do not appear in the spectra of the tetragonal compounds and they are assigned to  $\text{S}_3^{2-}$  bending and stretching modes respectively by analogy to  $\text{BaS}_3$  [30]. The weak bands at  $693\text{ cm}^{-1}$  is

assigned to a P–O mode by comparison with  $\text{P}_4\text{O}_6\text{S}$  and many other phosphorous oxysulfides [31] (P–O at  $726\text{ cm}^{-1}$  and P–O–P at  $640\text{ cm}^{-1}$ ).

#### 4. Concluding remarks

The system  $A_2\text{S}/\text{Pd}/\text{P}_2\text{S}_5$  has given rise to several interesting and intriguing compounds namely  $\text{K}_4\text{Pd}(\text{PS}_4)_2$  and  $\text{KPdPS}_4$  (already described) and now  $\text{NaPdPS}_4$ ,  $\text{RbPdPS}_4$  and  $\text{RbPdPS}_4\{\text{Rb}_{0.33}\text{P}_{0.4}\text{S}_{2.23}\text{O}_x\}$ . A puzzling finding is the isostructural nature of the Na and Rb analogs and the departure of the K analog from this structural motif. This raises projections of the possible existence of a second form of  $\text{KPdPS}_4$  that should be isostructural with the Na and Rb compounds. The isolation of this phase should be sought in future studies. Also surprising is the existence of cubic  $\text{RbPdPS}_4\{\text{Rb}_{0.33}\text{P}_{0.4}\text{S}_{2.23}\text{O}_x\}$  which forms under polythiophosphate flux conditions. The presence of molecular species such as  $\text{S}_3^{2-}$  and  $[\text{P}_4\text{S}_6\text{O}]^{6+}$  extracted for the flux medium betrays a templating effect tied to the size and shape of the cavity created by the packing of  $[\text{PdPS}_4]^-$  chains in cubic symmetry (or vice versa). Additional work is needed to better understand the nature of the encapsulated P–S–O species and corroborate its existence. Finally, these compounds dissolve in

Table 5  
Infrared and Raman spectra of II and III

Infrared			Raman		
RbPdPS <sub>4</sub>	RbPdPS <sub>4</sub> {Rb <sub>0.33</sub> P <sub>0.4</sub> S <sub>2.23</sub> O <sub>x</sub> }	KPdPS <sub>4</sub>	RbPdPS <sub>4</sub>	RbPdPS <sub>4</sub> {Rb <sub>0.33</sub> P <sub>0.4</sub> S <sub>2.23</sub> O <sub>x</sub> }	KPdPS <sub>4</sub>
239	233	240 $\delta(\text{PdS}_4)$		85	?
266	264	267 $\delta(\text{PS}_4)^{3-} + \delta(\text{SKS})$		122	?
302	310	311 $\delta(\text{PdS}_4) + \delta(\text{SKS})$	157	149	156 $R(\text{PS}_4)^{3-} + \delta(\text{PdS}_4) + \delta(\text{SKS})$
322		324 $\delta(\text{PS}_4)^{3-} + \nu_{\text{asym}}(\text{PdS}_4) + T_z(\text{K}_+)$		193	?
413		418 $\nu_{\text{sym}}(\text{PS}_4)^{3-} + \delta(\text{PdS}_4)$	209	204	200 $T_{x,y}(\text{PS}_4)^{3-} + \delta(\text{PdS}_4)$
553–588	553–592	555–590 $\nu_{\text{asym}}(\text{PS}_4)^{3-}$		216–237	$\delta(\text{S}_3^{2-})$
				257	?
			301	295	307 $\delta_{\text{asym}}(\text{PS}_4)^{3-} + \delta(\text{SKS})$
			328	324	324 $\delta(\text{PS}_4)^{3-} + \nu(\text{PdS}_4)$
			344	343	346 $\nu_{\text{sym}}(\text{PdS}_4)$
				382	?
			421	426	422 $\nu_{\text{sym}}(\text{PS}_4)^{3-} + \delta(\text{PdS}_4)$
				448–475	$\nu\text{S}_3^{2-}$
			556–600	560–617	555–599 $\nu_{\text{asym}}(\text{PS}_4)^{3-}$
				693	$\nu_{\text{asym}}(\text{P–O})$

strongly polar solvents leaving the  $[\text{PdPS}_4]^-$  chains intact, albeit in NMF for a limited time. The fresh solutions generate birefringent properties and complex fluid behavior due the organization of the very long chains in solution. Complex fluids, which include primarily organic polymeric and surfactant solutions as well as colloidal suspensions, are of universal industrial importance due to their unique mechanical properties, their capacity to solubilize and transport materials and their internal microstructures. Complex fluids composed of entirely inorganic species are rare and may have unique properties, however, they have been little investigated. The  $\text{APdPS}_4$  group of compounds could provide an interesting set of materials in which complex fluid behavior in non-oxidic, chalcogenide polymer systems may be investigated in the detail.

### Acknowledgment

Financial support from the National Science Foundation (DMR-0127644) is gratefully acknowledged.

### References

- [1] (a) M. Evain, R. Brec, G. Ouvrard, J. Rouxel, *J. Solid State Chem.* 56 (1985) 12–20.  
(b) S. Coste, E. Kopnin, M. Evain, S. Jobic, C. Payen, R. Brec, *J. Solid State Chem.* 162 (2001) 195–203.  
(c) M. Evain, M. Queignec, R. Brec, J. Rouxel, *J. Solid State Chem.* 56 (1985) 148–157.  
(d) E. Durand, M. Evain, R. Brec, *J. Solid State Chem.* 102 (1993) 146–155.
- [2] (a) J. Angenault, X. Cieren, G. Wallez, M. Quarton, *J. Solid State Chem.* 153 (2000) 55–65.  
(b) X. Cieren, J. Angenault, J.-C. Couturier, S. Jaulmes, M. Quarton, F. Robert, *J. Solid State Chem.* 121 (1996) 230–235.  
(c) E.-Y. Goh, E.-J. Kim, S.-J. Kim, *J. Solid State Chem.* 160 (2001) 195–204.  
(d) R.F. Hess, P.L. Gordon, C.D. Tait, K.D. Abney, P.K. Dorhout, *J. Am. Chem. Soc.* 124 (7) (2002) 1327–1333.  
(e) P.M. Briggs Piccoli, K.D. Abney, J.D. Schoonover, P.K. Dorhout, *Inorg. Chem.* 40 (19) (2001) 4871–4875.  
(f) C.R. Evenson, P.K. Dorhout, *Inorg. Chem.* 40 (12) (2001) 2884–2891.
- [3] T. McCarthy, M.G. Kanatzidis, *J. Alloys Compd.* 236 (1996) 70–85.
- [4] (a) K. Chondroudis, M.G. Kanatzidis, *Inorg. Chem.* 34 (1995) 5401–5402.  
(b) K. Chondroudis, M.G. Kanatzidis, *Inorg. Chem.* 37 (1998) 2098–2099.  
(c) P. Fragnaud, M. Evain, E. Prouzet, R. Brec, *J. Solid State Chem.* 102 (1993) 390–399.  
(d) K. Chondroudis, M.G. Kanatzidis, *J. Solid State Chem.* 136 (1998) 79–86.
- [5] M.G. Kanatzidis, *Cur. Opin. Solid State Mater. Sci.* 2 (1997) 139–149.
- [6] S. Coste, E. Kopnin, M. Evain, S. Jobic, R. Brec, K. Chondroudis, M.G. Kanatzidis, *Solid State Sci.* 4 (2002) 709–716.
- [7] S. Coste, M. Evain, E. Gauthier, R. Brec, S. Jobic, M.G. Kanatzidis, *Chem. Mater* 15 (12) (2003) 2323–2327.
- [8] S.H. Elder, A. Van der Lee, R. Brec, E. Canadell, *J. Solid State Chem.* 116 (1995) 107–112.
- [9] K. Chondroudis, M.G. Kanatzidis, J. Sayettat, S. Jobic, R. Brec, *Inorg. Chem.* 36 (1997) 5859–5868.
- [10] (a) J. Sayettat, L.M. Bull, J.C. Gabriel, S. Jobic, F. Camerel, A.-M. Marie, M. Fourmigué, P. Batail, R. Brec, R.-L. Inglebert, *Angew. Chem. Int. Ed.* 37 (1998) 1711–1714.  
(b) J. Sayettat, L.M. Bull, S. Jobic, J.C. Gabriel, M. Fourmigué, P. Batail, R. Brec, R.-L. Inglebert, C. Sourisseau, *J. Mater. Chem.* 9 (1999) 143–153.
- [11] (a) J.M. Tarascon, F.J. Disalvo, C.H. Chen, P.J. Carroll, M. Walsh, L. Rupp, *J. Solid State Chem.* 58 (1985) 290–300.  
(b) P. Davidson, J.C. Gabriel, A.M. Levelut, P. Batail, *Europhys. Lett.* 21 (1993) 317–322.
- [12] G.M. Sheldrick, *SHELXTLTM* version 5, Siemens analytical X-ray Instruments, Inc. Madison, WI.
- [13] V. Petricek, M. Dusek, *JANA 2000*, Institute of physics, Academy of sciences of the Czech Republic, Prague, Czech Republic, 2000.
- [14] P.E. Blöchl, *Phys. Rev. B* 50 (1994) 17953–17979.
- [15] G. Kresse, J. Joubert, *Phys. Rev. B* 59 (1999) 1758–1775.
- [16] (a) G. Kresse, J. Furthmüller, *Phys. Rev. B* 54 (1996) 11169–11186.  
(b) G. Kresse, J. Furthmüller, *Comput. Mater. Sci.* 6 (1996) 15–50.
- [17] P. Hohenberg, W. Kohn, *Phys. Rev. B* 136 (1964) 864–871.
- [18] W. Kohn, L.J. Sham, *Phys. Rev. B* 140 (1965) 1133–1138.
- [19] J.P. Perdew, Y. Wang, *Phys. Rev. B* 33 (1986) 8800.
- [20] O. Jepsen, O.K. Andersen, *Solid State Commun.* 9 (1971) 1763–1767.
- [21] G. Lehmann, M. Taut, *Phys. Status Solidi. B* 54 (1972) 469.
- [22] H.J. Monkhorst, J.D. Pack, *Phys. Rev. B* 13 (1976) 5188–5192.
- [23] S. Kashida, K. Nakamura, *J. Solid State Chem.* 110 (1994) 264–269.
- [24] E.R. Franke, H. Schafer, *Z. Naturforsch.* 27b (1972) 1308–1315.
- [25] S.S. Dhingra, R.C. Haushalter, *Chem. Mater.* 6 (12) (1994) 2376–2381.
- [26] (a) M.G. Kanatzidis, *Phosphorous, Silicon Sulfur* 93–94 (1994) 159–172.  
(b) K.-W. Kim, M.G. Kanatzidis, *J. Am. Chem. Soc.* 120 (32) (1998) 8124–8135.
- [27] (a) A.-F. Shihada, *Z. Naturforsch.* 48b (1993) 1781–1783.  
(b) U. Fleischer, F. Frick, A.R. Grimmer, W. Hoffbauer, M. Jansen, W. Kutzelnigg, *Z. Anorg. Allg. Chem.* 621 (1995) 2012–2020.
- [28] F. Camerel, Thesis, University of Nantes, 2001.
- [29] C. Sourisseau, R. Cavagnat, S. Jobic, R. Brec, *Chem. Phys.* 30 (1999) 721–731.
- [30] G.J. Janz, E. Roduner, J.W. Coutts, J.R. Downey, *Inorg. Chem.* 15 (8) (1976) 1751–1754.
- [31] A.R.S. Valentim, B. Engels, S. Peyerimhoff, J. Clade, M. Jansen, *Inorg. Chem.* 36 (1997) 2451–2457.